



HAL
open science

Intracellular Ca-carbonate biomineralization is widespread in cyanobacteria.

Karim Benzerara, Ferial Skouri-Panet, Jinhua Li, Céline Férard, Muriel Gugger, Thierry Laurent, Estelle Couradeau, Marie Ragon, Julie Cosmidis, N. Menguy, et al.

► **To cite this version:**

Karim Benzerara, Ferial Skouri-Panet, Jinhua Li, Céline Férard, Muriel Gugger, et al.. Intracellular Ca-carbonate biomineralization is widespread in cyanobacteria.. Proceedings of the National Academy of Sciences of the United States of America, 2014, 111 (30), pp.10933-8. 10.1073/pnas.1403510111 . hal-01101603

HAL Id: hal-01101603

<https://hal.sorbonne-universite.fr/hal-01101603>

Submitted on 9 Jan 2015

HAL is a multi-disciplinary open access archive for the deposit and dissemination of scientific research documents, whether they are published or not. The documents may come from teaching and research institutions in France or abroad, or from public or private research centers.

L'archive ouverte pluridisciplinaire **HAL**, est destinée au dépôt et à la diffusion de documents scientifiques de niveau recherche, publiés ou non, émanant des établissements d'enseignement et de recherche français ou étrangers, des laboratoires publics ou privés.

Classification:

Physical Sciences - Earth, Atmospheric, and Planetary Sciences; Biological Sciences – Microbiology

Intracellular Ca-carbonate biomineralization is widespread in cyanobacteria

Short title: *Intracellular Ca-carbonate in cyanobacteria*

Karim Benzerara^{a,1}, Feriel Skouri-Panet^a, Jinhua Li^a, Céline Féraud^a, Muriel Gugger^b, Thierry Laurent^b, Estelle Couradeau^{a,c}, Marie Ragon^{a,c}, Julie Cosmidis^a, Nicolas Menguy^a, Isabel Margaret-Oliver^a, Rosaluz Tavera^d, Purificacion Lopez-Garcia^c, David Moreira^c

^a Institut de Minéralogie, de Physique des Matériaux, et de Cosmochimie (IMPMC). Sorbonne Universités - UPMC Univ Paris 06, CNRS UMR 7590, MNHN, IRD UMR 206, 4 Place Jussieu, 75005 Paris, France

^b Institut Pasteur, Collection des Cyanobactéries, 75724 Paris Cedex 15, France

^c Unité d'Ecologie, Systématique et Evolution, CNRS UMR 8079, Université Paris-Sud, 91405 Orsay Cedex, France

^d Departamento de Ecología y Recursos Naturales, Universidad Nacional Autónoma de México, DF México, México

¹Corresponding author:

Dr. Karim Benzerara,

Institut de Minéralogie et de Physique de la Matière Condensée,

Case 115

4 Place Jussieu

75005 Paris, France;

Phone: 33-1-44277542

Email: karim.benzerara@upmc.fr

Keywords: biomineralization, controlled, Amorphous Calcium Carbonate, cyanobacteria, intracellular

Abstract (<250 mots)

Cyanobacteria have played a significant role in the formation of past and modern carbonate deposits at the surface of the Earth using a biomineralization process which has been almost systematically considered as induced and extracellular. Recently, a deep-branching cyanobacterial species, *Candidatus Gloeomargarita lithophora*, was reported to form intracellular amorphous Ca-rich carbonates, indicating the occurrence of controlled carbonate biomineralization. However, the significance and diversity of the cyanobacteria in which intracellular biomineralization occurs remain unknown. Here, we searched for intracellular Ca-carbonate inclusions in 68 cyanobacterial strains distributed throughout the phylogenetic tree of cyanobacteria. We discovered that diverse unicellular cyanobacterial taxa form intracellular amorphous Ca-carbonates with at least two different distribution patterns suggesting the existence of at least two distinct mechanisms of controlled biomineralization: i) one with Ca-carbonate inclusions scattered within the cell cytoplasm such as in *Ca. G. lithophora*, and ii) another one observed in strains belonging to the *Thermosynechococcus elongatus* BP-1 lineage, in which Ca-carbonate inclusions lie at the cell poles. This pattern seems to be linked with the nucleation of the inclusions at the septum of the cells, showing an intricate and original connection between cell division and biomineralization. These findings indicate that intracellular Ca-carbonate biomineralization by cyanobacteria has been overlooked by past studies and open new perspectives on the mechanisms and the evolutionary history of intra- and extra-cellular Ca-carbonate biomineralization by cyanobacteria.

Significance statement (120 word maximum)

Cyanobacteria are known to promote the precipitation of Ca-carbonate minerals by the photosynthetic uptake of inorganic carbon. This has resulted in the formation of carbonate deposits and a fossil record of importance for deciphering the evolution of cyanobacteria and their impact on the global carbon cycle. Yet the mechanisms of cyanobacterial calcification remain poorly understood, although this process is invariably thought as extracellular and the indirect byproduct of metabolic activity. Here, we show that contrary to common belief several cyanobacterial species control Ca-carbonate biomineralization intracellularly. We observed at least two phenotypes for intracellular biomineralization, one of which shows an original connection with cell division. These findings open new perspectives on the evolution of cyanobacterial calcification.

Introduction

Cyanobacteria are a phylogenetically and ecologically diverse phylum of Gram-negative bacteria, which have impacted the global cycle of carbon on the Earth for billions of years and induced the oxygenation of the atmosphere (1-3). By performing oxygenic photosynthesis, which is a unique capability that appeared only once in evolution, in this particular group of bacteria, they have contributed significantly to the primary production on the past and present Earth (4). Moreover, they have received great attention from geologists as major players in the formation of carbonate sedimentary deposits such as stromatolites (5, 6), the oldest ones formed by cyanobacteria being possibly as old as 2.98 Ga (7). Fossils of Ca-carbonate-encrusted cyanobacterial cells (calcimicrobes) have been looked for extensively. The temporal distribution of calcimicrobes in the geological record dating back as far as the early Proterozoic (~2.5-2.3 Ga, 8) has been interpreted as the result of paleoenvironmental (9) and/or evolutionary (10) changes. Despite the importance of carbonate biomineralization by cyanobacteria in the formation of calcimicrobes and sedimentary deposits, the involved mechanisms are yet poorly understood (e.g., 11, 12). Some authors have proposed that cyanobacterial calcification might be promoted by CO₂-concentrating mechanisms (CCMs) that possibly developed in the late Proterozoic to accommodate photosynthetic carbon limitation under low CO₂ fugacity (10). This model states that bicarbonates are actively imported into the cells, transformed to CO₂ within carboxysomes for fixation by RuBisCO. The resulting alkalinity is transferred outside the cells, which raises the external pH and thus induces CaCO₃ precipitation (13). In contrast, other authors found that some cyanobacteria induce CaCO₃ precipitation with no notable effect of photosynthesis and therefore stressed alternatively on the importance of cell surface properties for the nucleation of minerals (14). In any case, precipitation of CaCO₃ by cyanobacteria has been invariably considered as a non-controlled and extracellular process.

This paradigm has been questioned recently by the discovery of a new deep-branching cyanobacterial species, *Candidatus Gloeomargarita lithophora*, enriched from the hyperalkaline Lake Alchichica (Mexico) and forming amorphous carbonates intracellularly (15). Yet, many studies characterized the ultrastructure of cyanobacteria (e.g., 16, 17) and explored their impact on calcification (e.g., 11, 18, 19), but none of them reported the presence of intracellular carbonates. Here, we investigated whether intracellular carbonate biomineralization is restricted to one particular species and/or specific environmental conditions or whether it exists in other diverse cyanobacteria. This is essential to assess the evolution of intracellular carbonate biomineralization and its significance at geological timescales. For this purpose, we screened 68 cyanobacterial strains scattered throughout the phylogenetic tree of Cyanobacteria (Figure 1) to search for intracellular carbonates.

Results and discussion

Sixty-eight strains of cyanobacteria were imaged by scanning electron microscopy (SEM) using an angle selective backscattered electron (AsB) detector, which provides a chemical contrast. Their elemental composition was further analyzed by energy dispersive x-ray spectrometry (EDXS) coupled with SEM. Names of the strains, their geographic origin and the culture medium in which they were cultured are provided in Table S1. Most of the strains were obtained from culture collections (notably the Pasteur Culture Collection of Cyanobacteria) but we also studied a few other strains, in particular two strains that were isolated recently from microbialites from the alkaline Lake Alchichica (Mexico): *Ca. G. lithophora* (15) and a new species distantly related to *Thermosynechococcus elongatus* BP-1, which we have provisionally called *Candidatus Synechococcus calcipolaris* strain G9. Cyanobacteria have been classically grouped by subsections, defined on the basis of morphological and cell division features (e.g.,

20, 21). We covered all the subsections, with 26 strains belonging to subsection I, 5 to subsection II, 23 to subsection III, 10 to subsection IV and 4 to subsection V.

All but 8 of the tested strains showed intracellular inclusions as detected by SEM with a size range from ~100 up to 800 nm in diameter (SI Appendix, Table S1 and Fig. S1). Some strains contained numerous inclusions (e.g., PCC 73106, PCC 6308), while others had only one (e.g., PCC 7376) or two (e.g., PCC 7421) inclusions per cell. In some cases, these inclusions were preferentially located at the poles or showed alignments (e.g., PCC 7002, PCC 7429). These inclusions were in most cases composed of P as the major element with some Mg and K and sometimes Ca (SI Appendix, Fig. S2). According to their size, chemical composition and distribution patterns, they were interpreted as polyphosphate (PolyP) granules. In the past, PolyP granules have been identified by microscopy in many bacterial species, including some of the cyanobacterial strains analyzed in the present study (e.g., 22, 23). Such granules have sometimes been named metachromatic granules, or “volutin” (e.g., 17) and constitute a storage form of P for the cells or as a source of energy under P-limited or stress conditions (24).

The most striking result of this systematic survey was the discovery of seven cyanobacterial strains forming spherical and poorly crystalline intracellular carbonates (Fig. 2, 3, 4 and Table S2) in addition to *Ca. G. lithophora*, which was recently described (15). These strains were further analyzed by scanning transmission electron microscopy (STEM) in the high angular annular dark field (HAADF) mode which provides a chemical contrast with a higher spatial resolution compared to SEM. All these strains formed Mg- and K-containing PolyP granules as described above, but they also contained P-free, Ca-rich inclusions measuring between 60 and 870 nm in diameter and appearing as amorphous by electron diffraction, that we interpreted as Ca-carbonates (Fig. S2). The presence of Ca-carbonate inclusions was not dependent on the medium in which the strains were grown: first, several strains without Ca-carbonate inclusions were grown in BG11 similarly to the strains forming intracellular Ca-carbonates. Moreover,

Ca. G. lithophora D10 and *Ca. S. calcipolaris* G9 showed intracellular Ca-carbonate inclusions when grown in the different culture media (e.g., BG11_o or ASNIII) used for the other PCC strains screened in the present study (Fig. S3 and S4).

Two types of spatial distributions of the Ca-carbonate inclusions were observed:

Ca. G. lithophora D10, *Cyanothece* sp. PCC 7425 and *Chroococciopsis thermalis* PCC 7203 formed calcium carbonate inclusions scattered throughout the cell cytoplasm (Fig. 2). In *Cyanothece* sp. PCC 7425, most of the cells contained between 2 and up to 20 Ca-carbonate inclusions measuring between 130 and 700 nm. Few PolyP granules with no specific shape were observed, sometimes in very close spatial association with the Ca-carbonate inclusions (Fig. 2D). *Ca. G. lithophora* D10 cells contained between 3 and 19 Ca-carbonate inclusions measuring between 60 and 380 nm in diameter. They also contained PolyP granules larger and in higher number than *Cyanothece* sp. PCC 7425 cells (Fig. 2G). As a comparison, *Ca. G. lithophora* cells observed by Couradeau et al. (15) in laboratory aquaria which contained highly alkaline, Mg-rich and Ca, Sr and Ba-containing solutions contained no PolyP granule and a relatively higher number of carbonate inclusions enriched in Mg, Sr and Ba. The absence or presence of PolyP granules in *Ca. G. lithophora* cells can be explained by the very low vs. high orthophosphate contents of the laboratory aquaria vs. the BG11 medium, respectively, as shown previously for other strains (e.g., 24). In contrast, *Ca. G. lithophora* formed Ca-carbonate inclusions in laboratory aquaria as well as BG11 medium with some variations in their chemical composition (Mg, Sr and Ba content), likely depending on the concentration of these elements in the solutions. In *Chroococciopsis thermalis* PCC 7203 only few cells (baecytes and vegetative cells) showed between 8 and 20 Ca-carbonate inclusions per cell, measuring between 350 and 870 nm in diameter (Fig. 2A).

In contrast, *Synechococcus* sp. strains PCC6716, PCC6717, PCC6312, *Ca. S. calcipolaris* G9 and *Thermosynechococcus elongatus* BP-1 all showed Ca-carbonate inclusions clustered at the

cell poles and sometimes also in the middle of the cells (Fig. 3 and 4). The five strains showed very similar characteristics in terms of size, number and distribution patterns of the Ca-carbonate inclusion within the cells (Fig. 3 and 4). Cells contained between 5 and 40 inclusions at each pole, measuring between 90 and 300 nm in diameter. Inclusions in the middle of the cells were usually smaller, measuring between 50 and 150 nm in diameter. Overall, the numerous images that were acquired suggested that the formation of the Ca-carbonate inclusions is concomitant with the formation of the cell division septum (Fig. 4). After cell division, Ca-carbonate inclusions are therefore located preferentially at the poles of the cells. Controlled internal organizations of inclusions in cyanobacterial cells have been evidenced by several studies before. For example, PolyP granules are aligned in *Synechococcus* OS-B' (24), similarly to what was observed for many PCC strains here. Similarly, carboxysomes were shown to arrange along a similar linear organization in *Synechococcus elongatus* PCC 7942 (25) and to partition evenly between daughter cells. This non-random segregation and spatial organization is controlled and involves specific cytoskeletal proteins (25). Such a linear organization controlled by cytoskeletal proteins has also been observed in bacteria biomineralizing magnetites intracellularly (e.g., 26). Here, Ca-carbonate inclusions within the *T. elongatus* BP-1 group have a specific distribution within the cells as well, suggesting the existence of an original nucleation mechanism involving the cell cytoskeleton. Overall, this suggests that intracellular Ca-carbonate formation is a biologically controlled mineralization process (27).

It is interesting to note that PolyP granules were also observed in cells forming intracellular Ca-carbonate inclusions, sometimes in very close association with the Ca-carbonate inclusions (Fig 2). Formation of PolyP granules by PolyP kinases requires the sequestration of relatively high amounts of orthophosphate residues (e.g., 28) which have a strong inhibiting role on Ca-carbonate formation (e.g., 29). Moreover, there is a marked partitioning of Mg and K in the

PolyP granules vs. Ca in the carbonate inclusions. These observations show that strong chemical disequilibria or gradients are recorded within the cells by these mineral assemblages suggesting high confinement in the cytoplasm of the cells at the few nanometer-scale. Whether this involves membrane vesicles or not remains to be determined.

Moreover, intracellular Ca-carbonate biomineralization has been overlooked in the past, even for strains that have been kept in culture collections for decades. This may be due to the association of PolyP granules with Ca-carbonate inclusions in cells cultured in orthophosphate-rich culture media such as BG11 and the difficulty to distinguish between these different types of inclusions unless analytical tools such as EDXS mapping are used. Several past studies have analyzed thoroughly the ultrastructure of some of the intracellularly calcifying strains studied here. For example, Porta et al. (16) used a combination of confocal laser scanning microscopy and TEM to describe the ultrastructure of *Cyanothece* sp. PCC 7425. Interestingly, they mentioned the unusually high content of light refractile inclusions when viewed by phase-contrast microscopy but did not conclude on their chemical composition. Similarly, *T. elongatus* BP-1 has been used as a model for crystallographic studies of protein complexes such as photosystems, but intracellular Ca-carbonates had never been mentioned before for this strain. Therefore, there is a need for a systematic re-assessment of the presence/absence of Ca-carbonate inclusions in all cyanobacterial strains following a procedure similar to that shown here. In our study, cyanobacterial strains that do not form intracellular Ca-carbonates represent the majority. However, we show that intracellular Ca-carbonate biomineralization is not a rare capability. It is performed by strains isolated from diverse environments in various geographical sites, including a German soil, a rice field in Senegal, an alkaline lake in Mexico and hot springs in Japan and the USA (Oregon and Yellowstone) (Table S2).

Since the genome sequences of some of the strains analyzed here, in particular some intracellular Ca-carbonate-forming strains (PCC 6716, 6717, D10 and G9) are not available yet,

we used 16S rDNA sequences to study the phylogeny of these strains (Fig. 1) It is known that phylogenomic approaches provide a higher phylogenetic resolution than 16S rDNA-based methods but Shih et al. (20) noted the relatively good congruency between the two methods in the case of Cyanobacteria. Based on Figure 1 and Shih et al. (20) multi-gene phylogeny, it can be noted that intracellular Ca-carbonate biomineralization is phylogenetically fairly widespread in some (but not all) early-diverging phyla. For example, all 5 members of the *T. elongatus* BP-1 clade, which appears as an early branch of the cyanobacterial phylum (30), form intracellular Ca-carbonate inclusions suggesting that their ancestor had this capability as well. Reconstructing the timing of cyanobacteria evolution remains a challenge, in particular because of the existence of lateral gene transfers (e.g., 31) and the lack of reliable fossil evidence to date increasingly old nodes within the group (e.g., 1) but some tentative ages can be found in the literature. For example, the ancestor of the *T. elongatus* BP-1 clade was dated between ~2 and 2.5 Ga by Blank and Sanchez-Baracaldo (32). Although this is yet speculative, intracellular Ca-carbonate biomineralization may therefore have been an important biomineralization route in ancient cyanobacteria. The presence of Ca-carbonate inclusions in the very deep-branching species *Ca. G. lithophora* can be considered as an additional support for this idea.

Interestingly, whereas the pattern of Ca-carbonate inclusions limited to the cell poles is restricted to the *Thermosynechococcus* BP-1 clade, the three species containing inclusions scattered within the cell cytoplasm (*Ca. G. lithophora*, *Cyanothece* sp. PCC 7425, and *C. thermalis* PCC 7203) occupy very distant branches of the cyanobacterial tree (Fig. 1). There are two possibilities to explain this phylogenetic distribution: either this type of biomineralization was extremely ancient in Cyanobacteria and was lost in many lineages or it evolved several times independently in these three lineages. Moreover, phylogenomic analyses (20) supported that the *T. elongatus* BP-1 clade is sister to *Cyanothece* sp. PCC 7425 (their separation in our tree is most likely due to the limited phylogenetic signal of the 16S rDNA). If

this is confirmed, a single group would exhibit the two patterns of intracellular Ca-carbonate distribution. Since the cellular mechanism responsible for this controlled synthesis of Ca-carbonates remains unknown, it is difficult to distinguish between the hypotheses implying a single or several independent origins for this biomineralization capacity.

The relationship between intracellular and extracellular Ca-carbonate biomineralization will have to be investigated in the future. The formation of amorphous Ca-carbonate inclusions requires relatively high supersaturation conditions (e.g., 33) suggesting that relatively high concentrations of Ca^{2+} and/or CO_3^{2-} must prevail in the cytoplasm of intracellularly Ca-carbonate biomineralizing cyanobacteria. In general, some local increase in the concentration of CO_3^{2-} may be expected close to carboxysomes from which OH^- are released to the cytoplasm by the conversion of HCO_3^- to CO_2 by carboxysomal carbonic anhydrases (e.g., 34). Intracellular calcification may occur in Cyanobacteria regulating less efficiently their intracellular pH. Alternatively, regarding Ca^{2+} , it has been shown that free Ca^{2+} is highly regulated in the cytoplasm of living bacterial cells at a low concentration, including in some cyanobacteria (e.g., 35). Some variations can however occur, for example in response to stresses (e.g., 35), and it has been noted that they may have a physiological role and that cell division in particular appears very sensitive to the level of intracellular Ca^{2+} in *E. coli* (36). Interestingly, the present observations suggest that an increase of Ca^{2+} and/or CO_3^{2-} concentrations may occur specifically during cell division and locally near the septum in the strains of the *T. elongatus* BP-1 lineage as shown by the presence of Ca-carbonate inclusions. Whether some local Ca^{2+} influx related to cell division occurs in these strains will have to be tested. Finally, the possible existence of (specific or not) nucleation sites, and/or molecules stabilizing the amorphous Ca-carbonates and/or molecules inhibiting further Ca-carbonate growth after nucleation can be postulated to explain i) the discrete locations of Ca-carbonate inclusions, ii) the persistence of these unstable amorphous phases and iii) the fact that the cytoplasm does not get eventually

fully mineralized in these cells. In any case, such an intracellular biomineralization may lower at least partly the export outside the cell of the alkalinity generated by the photosynthetic activity and hence be detrimental to extracellular Ca-carbonate biomineralization. By sequestering at least transiently cytosolic inorganic carbon in solids, intracellular biomineralization may also interfere with the physiology of the cells. Recent studies of Ca-carbonate precipitation in cyanobacteria have been restricted to relatively few model strains, namely *Synechocystis* sp. PCC 6803 (e.g., 12, 37), *Synechococcus elongatus* PCC 7942 (e.g., 38), *Synechococcus* sp. PCC 8806 and *Synechococcus* sp. PCC 8807 (e.g., 18, 19). As shown here, *Synechocystis* sp. PCC 6803 does not form intracellular Ca-carbonate inclusions in BG11. *Synechococcus elongatus* PCC 7942 and *Synechococcus* sp. PCC 8806, previously observed using appropriate techniques (19, 38), do not form intracellular Ca-carbonate inclusions as well and can thus be considered as good models to study extracellular biomineralization of Ca-carbonate. Here, alternatively, new models for the study of intracellular biomineralization of Ca-carbonate are provided, offering a key to better understand the mechanisms governing the interactions between cyanobacteria and calcification by elucidating the molecular differences between these different patterns of biomineralization.

Materials and Methods

Strains and culture conditions. Sixty-four axenic strains were available from the Pasteur culture collection of Cyanobacteria (PCC strains, 20). They were axenic and have been described and studied by Rippka et al. (21) and Shih et al. (20). Culture media used for the different strains are reported in Table S1. Strains isolated from freshwater, soil or thermal environments were cultured in medium BG-11 and its variants, while marine strains were cultured in the more saline medium ASN-III and its variants (Table S1; 21). Recipes of the culture media are available on <http://cyanobacteria.web.pasteur.fr/>. All PCC cultures were

grown at 22°C except PCC 6716, 6717, 9339, 9431 and 9605 which were grown at 37°C. An axenic *Thermosynechococcus elongatus* strain BP-1, isolated from a hot spring in Beppu (Japan), was provided by Alain Boussac (CEA Saclay, France) and was cultured at 37°C in BG11. 1 non-axenic strain was an enrichment from Yellowstone. 2 non-axenic strains were enriched from Lake Alchichica. *Ca. G. lithophora* D10 was previously enriched and described in Couradeau et al. (15). A second strain was enriched following the same protocol. Because this strain was phylogenetically relatively distant from *Synechococcus* sp. PCC 6312, PCC 6716 and PCC 6717, and because it was enriched from a mesophilic environment on the contrary to *Thermosynechococcus elongatus* BP-1, we propose the following status for this new strain enriched from Lake Alchichica: order Chroococcales, *Ca. S. calcipolaris* sp. nov. Both cultures of *Ca. G. lithophora* D10 and *Ca. S. calcipolaris* G9 were grown in BG11 at 22°C.

Microscopy sample preparation. 0.5 mL of cultures were centrifuged at 8000 g for 10 min. Pellets were rinsed three times in mQ water. After the final centrifugation, pellets were resuspended in 200 µL. A drop of 5 µL was deposited on a carbon-coated 200-mesh copper grid and let dry at ambient temperature.

Electron microscopy analyses. SEM observations were performed on a Zeiss Supra 55 SEM microscope at a 10 kV working voltage with a working distance of 7.5 mm, an aperture of 60 µm and at high current. SEM images were collected with the Angle selective Backscattered (AsB) detector. Elemental maps of Ca, P and C were retrieved from hyperspectral images (Hypermap) consisting in an energy dispersive x-ray spectrometry (EDXS) analysis for each pixel of the image. Some strains, especially those forming intracellular Ca-carbonates, were further analyzed by TEM using a JEOL-2100F microscope operating at 200 kV, equipped with a field emission gun, a JEOL detector with an ultrathin window allowing detection of light elements, and a scanning TEM (STEM) device, which allows Z-contrast imaging in the high

angle annular dark field (HAADF) mode. Compositional mapping was acquired by performing EDXS analysis in the STEM HAADF mode.

Phylogenetic analysis. Genomic DNA was extracted from an enriched culture of *Ca. S. calcipolaris* with the PowerBiofilm® DNA Isolation Kit (MoBio) and used for 16S rRNA gene PCR amplification with the specific cyanobacterial primers CYA106F (CGGACGGGTGAGTAACGCGTGA) and 23S30R (CTTCGCCTCTGTGTGCCTAGGT). PCR reactions were carried out with 30 cycles (each one including denaturation at 94 °C for 15 s, annealing at 55 °C for 30 s, and extension at 72 °C for 2 min), preceded by 2 min denaturation at 94 °C, and followed by 7 min extension at 72 °C. PCR products were directly sequenced by Beckman Coulter Genomics (Takeley, United Kingdom) using the Cya106F forward primer and the 1492R (GGTTACCTTGTTACGACTT) as reverse universal primer for bacteria. The other cyanobacterial 16S rRNA gene sequences were retrieved directly from GenBank (<http://ncbi.nlm.nih.gov/>). Sequences were aligned using MAFFT (39) and the conserved sites were identified using Gblocks (40). Bayesian phylogenetic analysis was done using MrBayes 3.2.2 (41) with the general time reversible (GTR) model of sequence evolution, and taking among-site rate variation into account by using an eight-category discrete approximation of a Γ distribution and a proportion of invariant sites. Two parallel MCMC runs with four chains each (3 hot and 1 cold) were performed for 10 million generations and sampled every 10,000 generations, discarding a burnin of 25% before constructing a consensus tree. The 16S rRNA gene sequence of *Ca. S. calcipolaris* has been submitted to GenBank under accession number xxxx.

ACKNOWLEDGMENTS

The research leading to these results has received funding from the European Research Council under the European Community's Seventh Framework Programme (FP7/2007-2013 Grant Agreement no.307110 - ERC CALCYAN). The Pasteur culture collection of Cyanobacteria and MG and TL are funded by the Institut Pasteur. The SEM facility at IMPMC was purchased owing to a support by Région Ile de France grant SESAME 2006 I-07-593/R. The TEM facility at IMPMC was purchased owing to a support by Region Ile-de-France grant SESAME 2000 E 1435.

References

1. Tomitani A, Knoll AH, Cavanaugh CM, Ohno T (2006) The evolutionary diversification of cyanobacteria: Molecular-phylogenetic and paleontological perspectives. *Proc Natl Acad Sci USA* 103(14): 5442–5447.
2. Rosing MT, Bird DK, Sleep NH, Glassley W, Albarede F (2006) The rise of continents—An essay on the geologic consequences of photosynthesis. *Palaeogeogr, Palaeoclimatol, Palaeoecol* 232(2-4): 99–113.
3. Buick R (2008) When did oxygenic photosynthesis evolve? *Phil. Trans. R. Soc. B* 363(1504): 2731-2743.
4. Jansson C, Northen T (2010) Calcifying cyanobacteria—The potential of biomineralization for carbon capture and storage. *Curr. Opin. Biotechnol.* 21(3): 365–371.
5. Golubic S, Lee SJ (1999) Early cyanobacterial fossil record: preservation, palaeoenvironments and identification. *Europ. J. Phycol.* 34(4): 339-348.

6. Altermann W, Kazmierczak J, Oren A, Wright DT (2006) Cyanobacterial calcification and its rock-building potential during 3.5 billion years of Earth history. *Geobiology* 4(3): 147–166.
7. Bosak T, Knoll AH, Petroff AP (2013) The meaning of stromatolites. *Annu Rev Earth Planet Sci* 41(5): 21-44.
8. Klein C, Beukes NJ, Schopf JW (1987) Filamentous microfossils in the early Proterozoic Transvaal Supergroup - their morphology, significance, and paleoenvironmental setting. *Precamb. Res.* 36(1): 81-94.
9. Arp G, Reimer A, Reitner J (2001) Photosynthesis-induced biofilm calcification and calcium concentrations in Phanerozoic oceans. *Science* 292(5522): 1701-1704.
10. Riding R (2006) Cyanobacterial calcification, carbon dioxide concentrating mechanisms, and Proterozoic–Cambrian changes in atmospheric composition. *Geobiology* 4(4): 299-316
11. Kamennaya NA, Ajo-Franklin CM, Northen T, Jansson C (2012) Cyanobacteria as biocatalysts for carbonate mineralization. *Minerals*, 2(2): 338-364.
12. Jiang HB, Cheng HM, Gao KS, Qiu BS (2013) Inactivation of Ca²⁺/H⁺ Exchanger in *Synechocystis* sp. Strain PCC 6803 Promotes Cyanobacterial Calcification by Upregulating CO₂-Concentrating Mechanisms. *Appl. Environ. Microbiol.* 79 (13), 4048–4055.
13. Merz M (1992) The biology of carbonate precipitation by cyanobacteria. *Facies* 26(1): 81-101.
14. Obst M, Wehrli B, Dittrich M (2009) CaCO₃ nucleation by cyanobacteria: laboratory evidence for a passive, surface-induced mechanism. *Geobiology* 7(3): 324-347.
15. Couradeau E, et al. (2012) An early-branching microbialite cyanobacterium forms intracellular carbonates. *Science* 336(6080): 459-462.

16. Porta D, Rippka R, Hernandez-Mariné (2000) Unusual ultrastructural features in three strains of *Cyanothece* (cyanobacteria). *Arch Microbiol* 173(2): 154-163.
17. Allen MM (1984) Cyanobacterial cell inclusions. *Ann Rev Microbiol* 38: 1-25.
18. Lee BD, Apel WA, Walton MR (2006) Calcium carbonate formation by *Synechococcus* sp. Strain PCC 8806 and *Synechococcus* sp. strain PCC 8807. *Bioresource Technol* 97(18): 2427–2434.
19. Liang A, Paulo C, Zhu Y, Dittrich M (2013) CaCO₃ biomineralization on cyanobacterial surfaces: Insights from experiments with three *Synechococcus* strains. *Colloids and Surfaces B: Biointerfaces* 111(11): 600– 608.
20. Shih PM, et al. (2013) Improving the coverage of the cyanobacterial phylum using diversity-driven genome sequencing. *Proc Natl Acad Sci USA* 110(3): 1053–1058.
21. Rippka R, Deruelles J, Waterbury JB, Herdman M, Stanier RY (1979) Generic Assignments, Strain Histories and Properties of Pure Cultures of Cyanobacteria. *J. General Microbiol* 111(3): 1-61.
22. Morohoshi T, et al. (2002) Accumulation of inorganic polyphosphate in *phoU* mutants of *Escherichia coli* and *Synechocystis* sp. strain PCC6803. *Appl. Env. Microbiol.* 68(8): 4107-4110.
23. Jacobson L, Halmann M (1982) Polyphosphate metabolism in the blue-green alga *Microcystis aeruginosa*. *J. Plankton Res* 4(3): 481-488.
24. Gomez-Garcia MR, et al. (2013) Role of Polyphosphate in Thermophilic *Synechococcus* sp from Microbial Mats. *J. Bact.* 195(15): 3309-3319.
25. Savage DF, Afonso B, Chen AH, Silver PA (2010) Spatially Ordered Dynamics of the Bacterial Carbon Fixation Machinery. *Science* 327(5970): 1258-1261.
26. Scheffel A, et al. (2006) An acidic protein aligns magnetosomes along a filamentous structure in magnetotactic bacteria. *Nature*, 440(7090): 110-114.

27. Weiner S, Dove PM (2003) An overview of biomineralization processes and the problem of the vital effect. *Rev. Mineral. Geochem.* 54: 1-29.
28. Omelon SJ, Grynopas MD (2008) Relationships between Polyphosphate Chemistry, Biochemistry and Apatite Biomineralization. *Chem Rev.* 108(11): 4694-4715.
29. Dove PM, Hochella F, Jr. (1993) Calcite precipitation mechanisms and inhibition by orthophosphate: In situ observations by Scanning Force Microscopy. *Geochim. Cosmochim. Acta* 57(3): 705–714.
30. Robertson BR, Tezuka N, Watanabe MM (2001) Phylogenetic analyses of *Synechococcus* strains (cyanobacteria) using sequences of 16S rDNA and part of the phycocyanin operon reveal multiple evolutionary lines and reflect phycobilin content. *Int J Syst Evol Microbiol* 51(3): 861-871.
31. Szollosi GJ, Boussau B, Abby SS, Tannier E, Daubin V (2012) Phylogenetic modeling of lateral gene transfer reconstructs the pattern and relative timing of speciations. *Proc Natl. Acad. Sci USA* 109(43): 17513-17518.
32. Blank CE, Sanchez-Baracaldo P (2010) Timing of morphological and ecological innovations in the cyanobacteria - a key to understanding the rise in atmospheric oxygen. *Geobiology* 8(1): 1-23.
33. Wang D, et al. (2012) Revisiting geochemical controls on patterns of carbonate deposition through the lens of multiple pathways to mineralization. *Faraday Discussions* 159: 371-386.
34. Rae BD, Long BM, Badger MR, Price GD (2013) Functions, compositions, and evolution of the two types of carboxysomes: polyhedral microcompartments that facilitate CO₂ fixation in Cyanobacteria and some Proteobacteria. *Microbiol Mol Biol Rev* 77(3): 357-379.

35. Barran-Berdon AL, Rodea-Palomares I, Leganes F, Fernandez-Pinas, F (2011) Free Ca^{2+} as an early intracellular biomarker of exposure of cyanobacteria to environmental pollution. *Anal Bioanal Chem* 400(4): 1015-1029.
36. Holland IB, Jones HE, Campbell AK, Jacq A (1999) An assessment of the role of intracellular free Ca^{2+} in *E. coli*. *Biochimie* 81(8-9): 901-907.
37. Han Z, et al. (2013) Precipitation of calcite induced by *Synechocystis* sp. PCC6803. *World J Microbiol Biotechnol.* 29(10): 1801–1811.
38. Obst M, et al. (2009) Precipitation of amorphous CaCO_3 (aragonite-like) by cyanobacteria: A STXM study of the influence of EPS on the nucleation process. *Geochim Cosmochim Acta* 73(14):4180-4198.
39. Katoh K, Misawa K, Kuma K, Miyata T (2002) MAFFT: a novel method for rapid multiple sequence alignment based on fast Fourier transform. *Nucleic Acids Res.* 30(14): 3059-3066.
40. Castresana J (2000) Selection of conserved blocks from multiple alignments for their use in phylogenetic analysis. *Mol Biol Evol.* 17(4): 540-552.
41. Ronquist F, et al. (2012) MrBayes 3.2: efficient Bayesian phylogenetic inference and model choice across a large model space. *Syst Biol.* 61(3): 539-542.

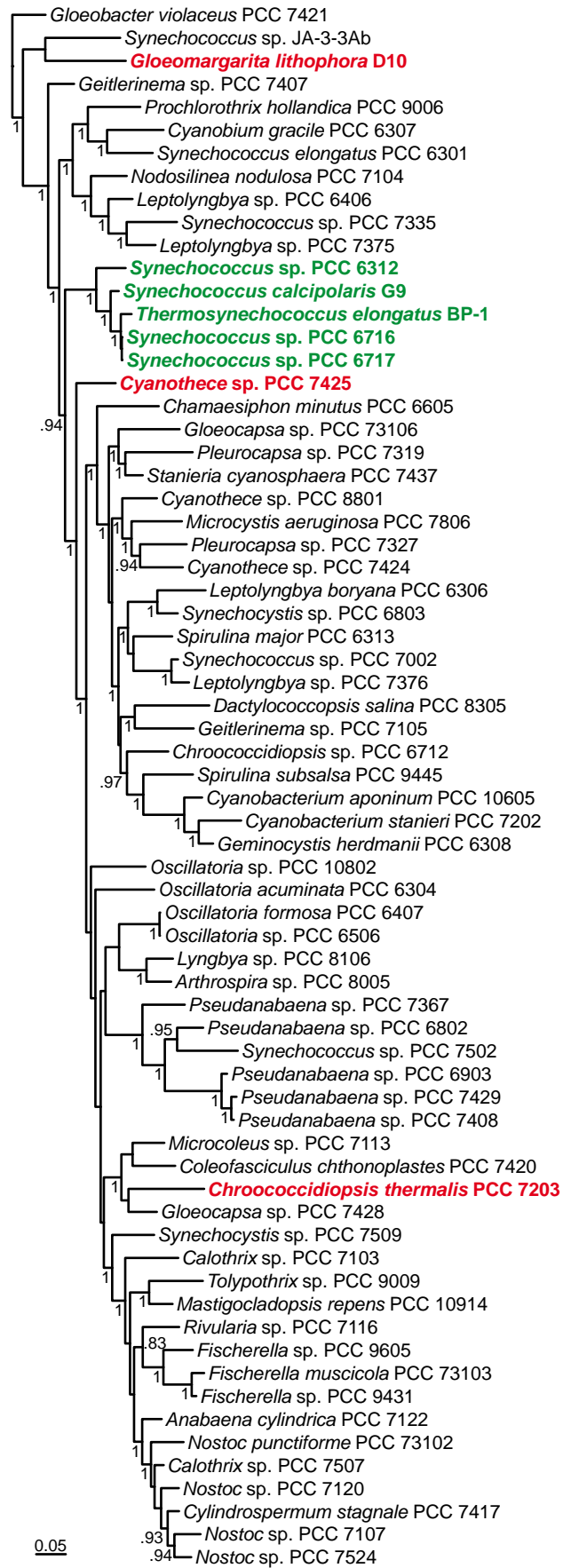
Figure Legends

Figure 1: Bayesian phylogenetic tree of 16S rRNA gene sequences of the cyanobacterial strains observed by electron microscopy. Strains forming intracellular Ca-carbonates are shown in color (green for those with Ca-carbonate inclusions at the cell poles and red for those with inclusions scattered in the cytoplasm). The tree is based on 1,292 conserved sites; numbers at branches are posterior probabilities (only those >0.75 are shown).

Figure 2: Electron microscopy images of cyanobacteria forming intracellular carbonates scattered throughout the cells. (A) and (B) SEM images in AsB detection mode of *Chroococcidiopsis thermalis* PCC 7203. (B) shows a baeocyte filled with Ca-carbonate inclusions. (C) STEM-EDX map of a vegetative cell of PCC 7203. (D) and (E) STEM-HAADF images of *Cyanothece* sp. PCC 7425. Ca-carbonate inclusions appear as bright round-shaped objects. PolyP granules are darker, sometimes shapeless forms (see arrows). (F) STEM-EDX map of PCC 7425. (G) and (H) STEM-HAADF images of *Ca. G. lithophora* strain D10. Ca-carbonates appear as brighter round-shaped inclusions, while PolyP granules are darker, sometimes bigger globules. PolyP granules sometimes seem to partly surround Ca-carbonate inclusions (see arrows). (I) STEM-EDX map of D10. The color code is the same for all STEM-EDX maps (C, F and I): Calcium is in green, phosphorus in red and carbon in blue. As a result, Ca-carbonates appear in green and PolyP granules in red.

Figure 3: Electron microscopy images of *Synechococcus* sp., *Ca. S. calcipolaris* and *Thermosynechococcus elongatus* strains forming intracellular carbonates. All of them form intracellular Ca-carbonates (brightest spots in STEM-HAADF images) located at the septum and the poles of the cells. (A) STEM-HAADF image (left) and EDX map (right) of *S. sp.* PCC 6716. Four aligned PolyP granules measuring ~500nm in diameter can be observed in the top cell (arrows). Clusters of 20 to 30 Ca-carbonate inclusions can be observed at both poles of the cell. (B) STEM-HAADF image and STEM-EDX map of strain PCC 6717 cell. (C) STEM-HAADF image and STEM-EDX map of *Ca. S. calcipolaris* G9 (Lake Alchichica). (D) STEM-HAADF image and STEM-EDX map of *Thermosynechococcus elongatus* BP1. The color code is the same for all STEM-EDX maps: Calcium is in green, phosphorus in red and carbon in blue.

Figure 4: STEM-HAADF images of *Synechococcus* sp. PCC 6312. Ca-carbonate inclusions were always observed at the poles of the cells and sometimes at the same location where septation occurs (arrows). Inclusions at the septum are usually smaller than at the poles. Division as observed in (B) and (D) seems to partition the Ca-carbonate inclusions between the daughter cells resulting in the polar distribution observed in all the cells. STEM-EDX map is shown in (C). Calcium is in green, phosphorus in red and carbon in blue.



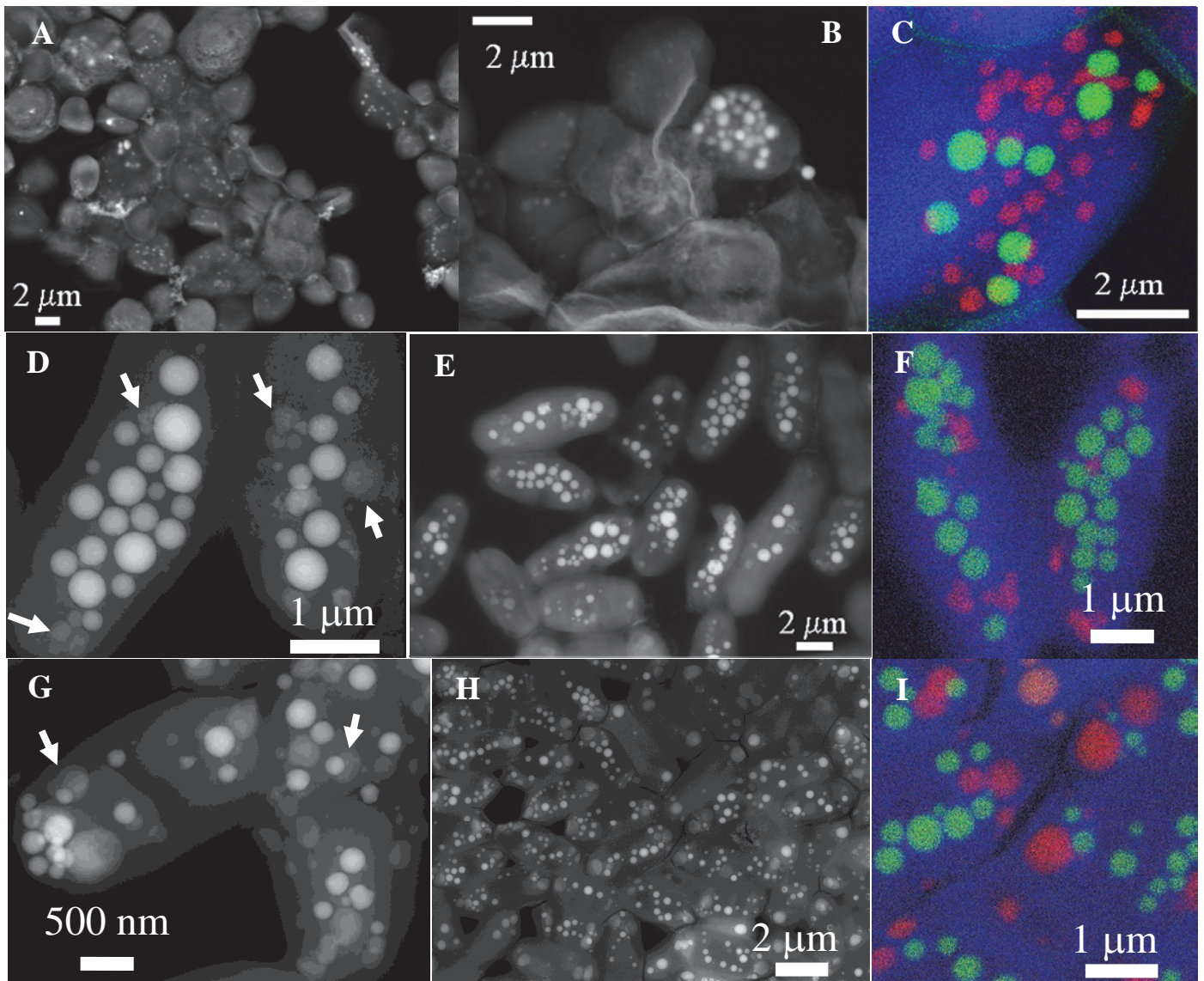


Figure 2. Electron microscopy images of cyanobacteria forming intracellular carbonates scattered throughout the cells. (A) and (B) SEM images in BSE mode of *Chroococcidiopsis thermalis* PCC 7203. (B) shows a baeocyte filled with Ca-carbonate inclusions. (C) STEM-EDX map of a vegetative cell of PCC 7203. (D) and (E) STEM-HAADF images of *Cyanotheca* sp. PCC 7425. Ca-carbonate inclusions appear as bright round-shaped objects. PolyP granules are darker, sometimes shapeless forms (see arrows). (F) STEM-EDX map of PCC 7425. (G) and (H) STEM-HAADF images of *Candidatus Gloeomargarita lithophora* strain D10. Ca-carbonates appear as brighter round-shaped inclusions, while PolyP granules are darker, sometimes bigger globules. PolyP granules sometimes seem to partly surround Ca-carbonate inclusions (see arrows). (I) STEM-EDX map of D10. The color code is the same for all STEM-EDX maps (C, F and I): Calcium is in green, phosphorus in red and carbon in blue. As a result, Ca-carbonates appear in green and PolyP granules in red.

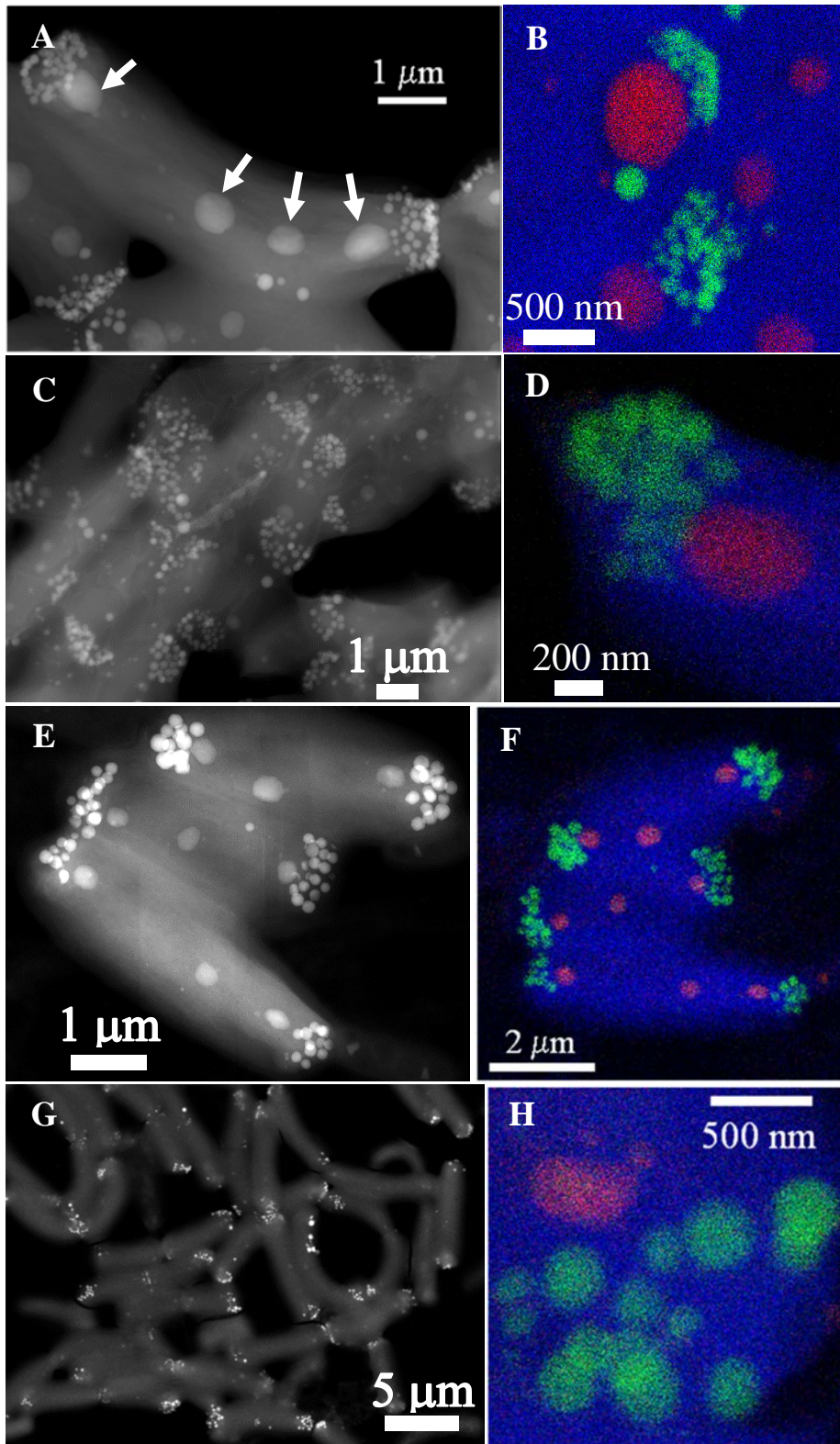


Figure 3: Electron microscopy images of *Synechococcus* sp., *Candidatus Synechococcus calcipolaris* and *Thermosynechococcus elongatus* strains forming intracellular carbonates. All of them form intracellular Ca-carbonates (brightest spots in STEM-HAADF images) located at the septum and the poles of the cells. (A) STEM-HAADF image and (B) EDX map of *S. sp.* PCC 6716. Four aligned PolyP granules measuring ~500nm in diameter can be observed in the top cell (arrows). Clusters of 20 to 30 Ca-carbonate inclusions can be observed at both poles of the cell. (C) STEM-HAADF image and (D) STEM-

EDX map of strain PCC 6717 cell. (E) STEM-HAADF image and (F) STEM-EDX map of *Candidatus Synechococcus calcipolaris* G9 (Lake Alchichica). (G) STEM-HAADF image and (H) STEM-EDX map of *Thermosynechococcus elongatus* BP1. The color code is the same for all STEM-EDX maps: Calcium is in green, phosphorus in red and carbon in blue.

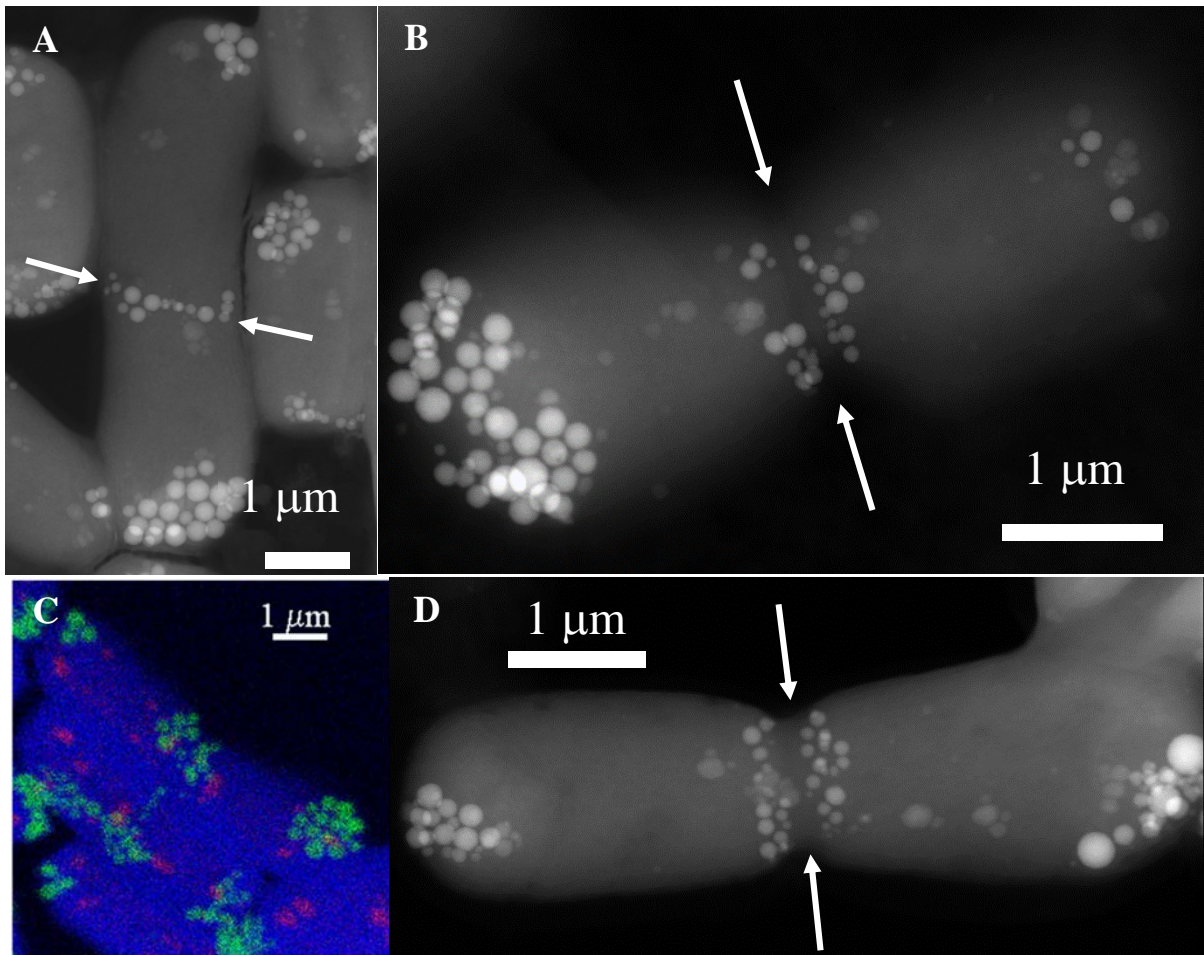


Figure 4: STEM-HAADF images of *Synechococcus* sp. PCC 6312. Ca-carbonate inclusions were always observed at the poles of the cells and sometimes at the same location where septation occurs (arrows). Inclusions at the septum are usually smaller than at the poles. Division as observed in (B) and (D) seems to partition the Ca-carbonate inclusions between the daughter cells resulting in the polar distribution observed in all the cells. STEM-EDX map is shown in (C). Calcium is in green, phosphorus in red and carbon in blue.